SIAM J. APPL. MATH.
Vol. 70, No. 7, pp. 2409–2433

THE MORPHOLOGY OF THE MARTIAN ICE CAPS: A MATHEMATICAL MODEL OF ICE-DUST KINETICS*

R. J. ZAMMETT† AND A. C. FOWLER‡

Abstract. Spiral-shaped canyons on the polar ice caps of Mars are striking morphological features whose explanation is still mysterious. We pose a model for the kinetics at the ice-atmosphere interface based on the positive feedback properties of both dust and ice albedo within the north polar ice cap, together with katabatic wind transport of exposed dust. Analysis of this model indicates that traveling waves are possible, but only solitary waves are found in the numerical solution. This suggests that the traveling wave hypothesis for trough formation may not be an appropriate explanation.

Key words. Mars, polar ice caps, spiral waves, phase plane analysis

AMS subject classifications. 70K05, 85A20, 86A10, 86A40

DOI. 10.1137/080734558

1. Introduction.

Mars has two polar ice caps, of which the larger is that in the north. Both polar caps exhibit strange spiral structures, particularly that in the north, as shown in Figure 1.1 (Blasius, Cutts, and Howard (1982)). These spirals are indications of a periodic winding sequence of canyons in the surface of the ice sheet, which are made visible because of the increased presence of exposed dust layers within the ice.

The north polar cap is considered to consist largely of water ice (Kieffer et al. (1976)), interspersed with a regular sequence of dust layers within the ice, thought to be due to irregular fluctuations in the past climate (for example, due to major planetary obliquity variations (Carr (1982), Cutts and Lewis (1982), Toon et al. (1980)). General descriptions of the layered deposits are given by Kieffer et al. (1976) and Thomas et al. (1992).

The characteristics of the northern ice cap spiral troughs have been described by Howard (1978), Howard, Cutts, and Blasius (1982), and more recently by Howard (2000). Figure 1.2 shows a cross-sectional profile through the ice cap. The dust layers within the ice are thought to be between 5 and 50 m thick, while the troughs themselves are spaced at typical intervals of 50 km (Carr (1982)). The troughs are separated by scarps which have slopes up to 5° and are up to 1000 m high and up to 10 km wide, but may be both smaller and narrower (Howard (1978)). Troughs are up to 1 km deep, between 5 and 30 km wide, and up to several hundred kilometers long (Thomas et al. (1992)). The scarps form the spiral pattern seen in Figure 1.1 and are visible because of their lower albedo, which is due to the higher dust fraction exposed by the steeper slopes.

There has been much interest in the origin of the spiral canyons, which are unlike anything known on Earth on either of the two major ice sheets of Antarctica and Greenland. Howard (1978) was the first to suggest a possible mechanism for their formation, the dust-albedo feedback hypothesis. This idea is based on the fact that south-

*Received by the editors September 5, 2008; accepted for publication (in revised form) January 12, 2010; published electronically June 23, 2010.
http://www.siam.org/journals/siap/70-7/73455.html
†Mathematical Institute, Oxford University, 24-29 St. Giles', Oxford OX1 3LB, UK (rachel_zammett@yahoo.co.uk). The work of this author was supported by an EPSRC studentship.
‡MACSI, University of Limerick, Limerick, Ireland (andrew.fowler@ul.ie). The work of this author was supported by the Mathematics Applications Consortium for Science and Industry (www.macsi.ul.ie) funded by Science Foundation Ireland mathematics initiative grant 06/MI/005.

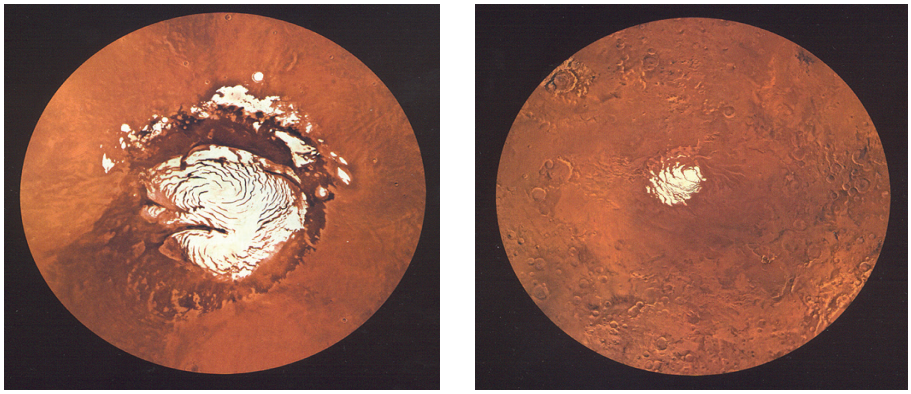

FIG. 1.1. *Aerial Viking Orbiter* 1 *images of the residual north and south polar ice caps (left and right, respectively) courtesy of NASA/JPL/USG; see http://photojournal.jpl.nasa.gov/catalog/PIA00190 and http://photojournal.jpl.nasa.gov/catalog/PIA00161. The photographs extend to* $65^\circ N$ *and* $60^\circ S$*, respectively. The north polar residual ice cap is about* 1000 *km in width at its maximum; the large re-entrant valley (Chasma Borealis) is located at* $300^\circ E$ *and is* 600 *km long. Thanks to Felix Ng for directing us to these images.*

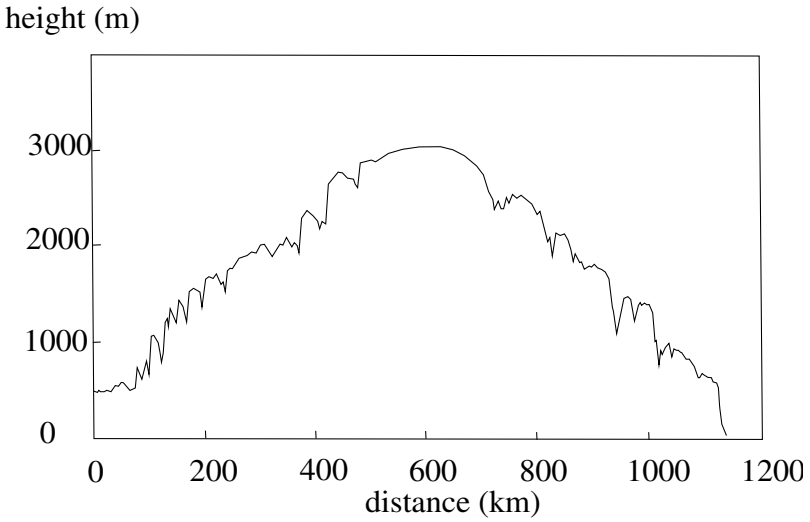

FIG. 1.2. *A cross section of the north polar ice cap, showing the scarps and canyons. Redrawn from Ivanov and Muhleman* (2000). *The height is relative to a plane* 5 *km below the mean geoid. The north pole is near the summit.*

facing scarps receive more solar radiation, and ice there will therefore preferentially sublimate, whereas on the cooler flats deposition will occur.[1] The resulting sublimation on the scarps exposes increased dust at the surface, and this decreases the albedo of the surface, thus increasing sublimation. This positive feedback is a possible instability mechanism and suggests the possibility of a bistable switching between sublimation and deposition of ice. This is then supposed to lead to the observed corrugations.

[1]The summer north polar temperature on Mars is about 200 K (Kieffer et al. (1976)), and melting does not occur.

Howard's idea has been explored by others, notably Ivanov and Muhleman (2000), who provided a mathematical basis for Howard's descriptive model based on a description of radiation imbalance at the surface. Ng and Zuber (2006) have used this to develop a more complete explanatory model which fully incorporates the dust-albedo feedback mechanism and transport of ice and atmospheric water vapor. Their model suggests that the troughs are evolving today from an ancient albedo imprint on the ice cap surface and provides the conceptual starting point for the present work.

The core idea that the spiral waves arise as an instability informs Ng and Zuber's model, and it also lies at the heart of Pelletier's (2004) theory. Pelletier uses a version of the Fitzhugh–Nagumo model to produce spiral waves. It is well known in the theory of reaction-diffusion equations (e.g., Murray (1993)) that the combination of oscillatory reaction kinetics with a diffusive transport mechanism leads to periodic traveling waves, and with a suitable central seeding mechanism either target patterns or spiral waves can be formed. Evidently, the radial symmetry of received solar radiation and/or the (approximate) symmetry of the ice cap will provide such a seeding mechanism on Mars, and the dust-albedo feedback mechanism may produce oscillatory kinetics. There then remains the issue of transport. Pelletier uses thermal diffusion of ice temperature, which does not appear tenable, and indeed the strength of Pelletier's theory lies in how it makes the connection with reaction-diffusion theory; the physical basis of both the kinetics and the transport of his model is questionable.

A number of authors, particularly Howard (1981, 2000), suggest that katabatic winds flowing down the ice cap will provide the necessary transport mechanism, and we follow this suggestion here. Despite a low atmospheric pressure of about 6 millibars (600 Pa), weather systems on Mars are strong (Leovy (2001)), and visual evidence of large dust storms shows directly that aeolian transport processes are effective. During the polar winter, temperatures sink to 140 K, and the polar cap is covered with a CO_2 frost, presumably preventing sediment transport. Elevated atmospheric temperatures in the summer suggest downslope katabatic winds, and evidence for these exists in wind streaks on the ice cap itself, and in the surrounding dune fields which are indicators of wind direction (Tsoar, Greeley, and Peterfreund (1979), Greeley et al. (1992)). Numerical simulations also suggest that downslope katabatic winds will be prevalent in summer (Tyler and Barnes (2005)).

Paucity of observations means that it is difficult to be definitive about processes which may occur on Mars, and there may be other important features to consider. In particular, the ice cap will flow, albeit very slowly (perhaps millimeters per year), and Fisher (1993, 2000) has used this as a basis for a description of the spirals (and other features, notably the large re-entrant chasmae which can be seen in Figure 1.1). Clifford (1987, 1993) has suggested that the large thickness of the layered deposits (some 4–6 km) and the resulting insulating effect may cause basal melting to occur, and that possibly the chasmae were formed through massive subglacial floods (jökulhlaups). While there is clear evidence of massive water flow on early Mars (Baker (2001)), it remains speculative whether subglacial floods of this type could have occurred from beneath the polar ice cap.

In this paper, we investigate the hypothesis that the troughs can be explained as traveling waves on the ice cap surface. We first use Ivanov and Muhleman's (2000) model of sublimation kinetics to derive a mathematical model that describes the kinetics of the interaction between ice and suspended atmospheric dust in the Martian north polar region. This model is nondimensionalized and solved. We then modify the original model to include transport terms in one dimension: ice transport by steady

state creep and atmospheric dust transport by a downslope katabatic wind. Possible traveling wave solutions of this model are investigated both analytically, using phase plane analysis, and numerically.

2. Kinetics of ice and dust. We begin by formulating a model for the kinetics of the interaction between the ice surface and the overlying atmosphere (see Figure 2.1). The constituent variables of the model will be the ice surface elevation h, the surface temperature T, atmospheric water vapor pressure p and density ρ_v, the atmospheric suspended dust concentration c, and the dust volume fraction ϕ in near surface ice. We define also a quantity α, which is the volume fraction of dust contained in atmospheric snow (supposing that accretion takes place by snowfall). This encapsulates the idea that snow will form by nucleation on suspended dust particles, as suggested by Pollack et al. (1979). We measure both ρ_v and c in units of kg m^{-3}, but ϕ and α are pure numbers, between 0 and 1. In this section we will ignore spatial variations and suppose that all these variables are functions of time t only.

The basis of the model is the radiation balance at the surface, described by Ivanov and Muhleman (2000). If I is the received short wave solar radiation at the top of the atmospheric column (which in general will allow for the effect of season and latitude as well as ice surface slope), then an energy balance at the ice surface takes the form

$$I(1-a) = \gamma\sigma T^4 + mL, \tag{2.1}$$

where m is the rate of sublimation (precisely, the rate of loss of water substance from the ice surface; $m < 0$ indicates accretion, for example, via snowfall) and L is the latent heat. The first term on the right is the black body long wave emitted radiation at the surface (see, for example, Liou (2002)), corrected for the greenhouse effect of

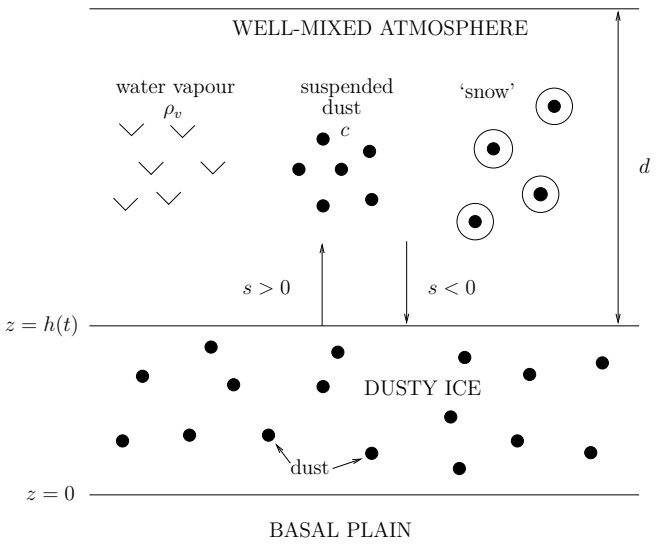

FIG. 2.1. *Schematic illustration of the kinetic processes on the ice cap. The atmosphere contains dust* (c) *and water vapor* (ρ_v) *or, when freezing, snow crystals nucleated on dust particles. Interchange occurs at the ice surface through sublimation* ($s > 0$) *or accretion* ($s < 0$), *thus releasing or burying the dust content of the ice* (ϕ). *Arrows at the surface denote movement of water ice/vapor: water ice sublimes into the atmosphere if* $s > 0$ *and accretes on the ice cap surface if* $s < 0$.

atmospheric dust by a factor $\gamma < 1$, and the incoming radiation is modified by a dusty ice albedo coefficient a. These coefficients depend on the dust content of the ice (a) and the dust content of the atmosphere (c); thus $a = a(\phi)$, $\gamma = \gamma(c)$, and a and γ are decreasing functions of ϕ and c. The idea here is that dusty ice reflects incoming short wave radiation, while a dusty atmosphere causes increased absorption of long wave radiation, and thus an increased surface temperature because of the greenhouse effect. The units of I are W m^{-2}, while those of L are J kg^{-1}, and therefore m has units of kg m^{-2} s^{-1}.

It is convenient to relate mass wastage to the rate of elevation of the ice surface, measured as a velocity. Suppose this is s. From the definitions of ϕ and α, we therefore have

$$m = \begin{cases} \rho_i(1-\phi)s, & s > 0, \\ \rho_i(1-\alpha)s, & s < 0, \end{cases} \tag{2.2}$$

where ρ_i is the density of ice. An expression for m has been given by Ivanov and Muhleman (2000). Sublimation will occur when the atmospheric water vapor pressure is less than the saturation vapor pressure, which we denote by $p_{\rm sat}$. Then Ivanov and Muhleman suggest that

$$m = D(p_{\rm sat} - p)\sqrt{\frac{m_w}{2\pi kT}}, \tag{2.3}$$

where k is Boltzmann's constant and m_w is the molecular mass of a water molecule. Ivanov and Muhleman further suggest that

$$D = Au\sqrt{\frac{2\pi m_w}{kT}}, \tag{2.4}$$

where u is the surface wind speed, and with this we have

$$m = \frac{Am_w u(p_{\rm sat} - p)}{kT}, \tag{2.5}$$

where A is an empirically determined pure number, which Ivanov and Muhleman (2000) tentatively suggest should be $A \approx 0.002$.

The saturation vapor pressure is determined from the solution of the Clausius–Clapeyron equation; this is

$$p_{\rm sat} = p_{\rm sat}^{\rm ref} \exp\left[B\left\{1 - \frac{T_{\rm ref}}{T}\right\}\right], \tag{2.6}$$

where $p_{\rm sat} = p_{\rm sat}^{\rm ref}$ at $T = T_{\rm ref}$, and the parameter B is given by

$$B = \frac{M_w L}{RT_{\rm ref}}, \tag{2.7}$$

where M_w is the molecular weight of water, and R is the perfect gas constant. In terms of the vapor pressure, the vapor density is given by the perfect gas law

$$\rho_v = \frac{M_w p}{RT}. \tag{2.8}$$

For the ten variables h, ρ_v, c, T, p, ϕ, α, m, s, and $p_{\rm sat}$, we have provided so far the five algebraic equations (2.1), (2.2), (2.5), (2.6), and (2.8); five further equations

are required. These consist of two constitutive equations for the dust fractions α and ϕ, and three conservation laws for ρ_v, c and h. We consider first the constitutive equations.

The most elusive is that for the ice dust fraction ϕ. This is easy enough if ice accretes through snowfall, that is, $s < 0$. We defined α to be the volume fraction of the snow particles occupied by dust. Then, if we suppose that no ice-free dust accumulates on the surface by settlement, we simply have

$$\phi = \alpha, \quad s < 0. \tag{2.9}$$

However, if sublimation is occurring, then the value of ϕ is equal to the value of α when the surface was last exposed. This leads us to define

$$\phi = \alpha(\tau), \quad s > 0, \tag{2.10}$$

where, since the elevation rate of the surface is simply $-s$, τ is defined by

$$\tau = \max\left\{t^* < t : \int_{t^*}^{t} s(t')\,dt' = 0\right\} \qquad \text{for } s > 0. \tag{2.11}$$

Therefore, if sublimation is occurring ($s > 0$) definition (2.11) indicates that $h(t) = h(\tau)$; i.e., the height of the ice cap surface is the same at times t and τ. We thus have the combined definition of ϕ as

$$\begin{cases} \tau = t, & \phi = \alpha(\tau), \\ & s < 0, \\ \tau = \max\left\{t^* < t : \displaystyle\int_{t^*}^{t} s(t')\,dt' = 0\right\}, & s > 0. \end{cases} \tag{2.12}$$

The dust volume fraction within snow particles, α, must be related to the atmospheric dust concentration c (since if $c = 0$, then clearly $\alpha = 0$). The definition of α is only relevant when it is snowing, i.e., $s < 0$. A simple assumption is then that ice nucleates on all dust particles so that $\alpha \propto c$, and the proportionality factor depends on our assumption about snow crystal growth rates. For example, suppose that vapor forms ice crystals rapidly, so that when $p > p_{\text{sat}}$, all the vapor crystallizes. Then the atmospheric volume fraction c/ρ_s of dust (where ρ_s is the density of dust) is locked into a volume fraction ρ_v/ρ_i of frozen vapor, so that

$$\alpha = \frac{c}{c + r_{si}\rho_v}, \tag{2.13}$$

where

$$r_{si} = \frac{\rho_s}{\rho_i} \tag{2.14}$$

is the ratio of dust to ice density. A more general assumption is that (2.13) provides an upper bound for α.

Finally, we have three conservation equations for h, ρ_v, and c. The simplest is that for the ice surface h, which is just

$$\frac{dh}{dt} = -s. \tag{2.15}$$

Conservation of atmospheric dust and water vapor in a column of height d implies

$$d\frac{d\rho_v}{dt} = \begin{cases} \rho_i(1-\phi)s, & s > 0, \\ \rho_i(1-\alpha)s, & s < 0, \end{cases} \tag{2.16}$$

and

$$d\frac{dc}{dt} = \begin{cases} \rho_s\phi s, & s > 0, \\ \rho_s\alpha s, & s < 0. \end{cases} \tag{2.17}$$

This completes this specification of the spatially independent model.

Complicated as it is, it is still an oversimplification. Two elaborations are worth considering. One is to include explicitly a variable describing atmospheric snow concentration. Implicitly (2.16) describes snow crystal growth and removal, but in so doing it prejudices a safe determination of α. Of course, snow may not occur, and accretion could occur directly at the surface. This highlights a second shortcoming of the model, for in that case $\alpha = 0$ and there is no mechanism for dust accretion to occur. In fact, (2.17) implicitly assumes that when ice sublimation occurs, the resulting exposed dust is instantly whisked up into the atmosphere, presumably by wind erosion; this suggests that a more elaborate model would treat the surface density of exposed dust as a separate variable.

2.1. Nondimensionalization. Our first task is to nondimensionalize these model equations. We scale the variables with quantities subscripted (or superscripted) by zero, and thus $T \sim T_0$, $m \sim m_0$, and so on; we thus have to choose scales for the eight dependent variables (other than ϕ and α, which are already dimensionless numbers between zero and one), together with a time scale t_0, and for future reference we also choose a velocity scale u_0 for the wind speed u. We choose the scales by balancing terms in the equations, and in fact we balance all the terms except the latent heat term in (2.1) and the terms in (2.16). We calculate a suitable scale for the insolation using spherical geometry, so that

$$I_0 = S\cos\theta_f = 128 \text{ W m}^{-2}, \tag{2.18}$$

where $S = 588$ W m^{-2} is the Martian solar constant and $\theta_f = 77.4^\circ$ is an average solar zenith angle for the residual north polar ice cap (see Zammett (2008)). Using this scale value for the insolation, we sequentially define the scales:

$$T_0 = \left[\frac{I_0(1-a_0)}{\sigma}\right]^{\frac{1}{4}}, \quad p_0 = p^0_{\text{sat}} = p^{\text{ref}}_{\text{sat}} \exp\left[B\left\{1 - \frac{T_{\text{ref}}}{T_0}\right\}\right], \quad m_0 = \frac{Am_w u_0 p^0_{\text{sat}}}{kT_0},$$
$$s_0 = \frac{m_0}{\rho_i}, \quad \rho^0_v = \frac{M_w p^0_{\text{sat}}}{RT_0}, \quad c_0 = r_{si}\rho^0_v, \quad t_0 = \frac{dc_0}{\rho_s s_0}, \quad h_0 = s_0 t_0. \tag{2.19}$$

TABLE 2.1
Parameter values.

Parameter	Meaning	Typical value
L	latent heat of sublimation of water ice	2.83×10^6 J kg^{-1}
R	perfect gas constant	8.31 J mol^{-1}K^{-1}
M_v	molar mass of water	1.80×10^{-2} kg mol^{-1}
σ	Stefan–Boltzmann constant	5.67×10^{-8} kg s^{-3} K^{-4}
A	turbulent drag coefficient	0.002
u_0	wind speed	5 m s^{-1}
m_w	molecular mass of water	2.99×10^{-26} kg
k	Boltzmann constant	1.38×10^{-23} J K^{-1}
d	depth of layer of mixed atmosphere	100 m
ρ_s	density of dust	2×10^3 kg m^{-3}
ρ_i	density of ice	900 kg m^{-3}
$p_{\text{sat}}^{\text{ref}}$	reference saturation vapor pressure	611 Pa
T_{ref}	reference temperature	273 K
a_0	average surface albedo	0.33
I_0	typical insolation	128 W m^{-2}

We then derive the dimensionless form of the model (dropping the subscript v on ρ_v):

$$
\begin{aligned}
I(1-a) &= \gamma T^4 + \lambda m,\\
m &= \begin{cases} (1-\phi)s, & s > 0,\\ (1-\alpha)s, & s < 0,\end{cases}\\
m &= \frac{|u|(p_{\text{sat}} - p)}{T},\\
p_{\text{sat}} &= \exp\left[\beta\left(1 - \frac{1}{T}\right)\right],\\
\rho &= \frac{p}{T},\\
\phi &= \alpha(\tau), \qquad \begin{cases} \tau = t, & s < 0,\\ \displaystyle\int_\tau^t s(t')\,dt' = 0, & s > 0,\end{cases}\\
\alpha &= \frac{c}{c+\rho},\\
\frac{dh}{dt} &= -s,\\
\frac{d\rho}{dt} &= \begin{cases} (1-\phi)s, & s > 0,\\ (1-\alpha)s, & s < 0,\end{cases}\\
\frac{dc}{dt} &= \begin{cases} \phi s, & s > 0,\\ \alpha s, & s < 0,\end{cases}
\end{aligned}
\tag{2.20}
$$

and the dimensionless parameters are defined by

$$
\beta = \frac{M_w L}{R T_0}, \quad \lambda = \frac{m_0 L}{\sigma T_0^4}. \tag{2.21}
$$

Using the parameter values given in Table 2.1, we calculate the following scales:

$$
\begin{gathered}
T_0 \approx 198 \text{ K}, \quad p_0 \approx 0.114 \text{ Pa}, \quad m_0 \approx 1.26 \times 10^{-8} \text{ kg m}^{-2} \text{ s}^{-1},\\
s_0 \approx 1.40 \times 10^{-11} \text{ m s}^{-1}, \quad \rho_0 \approx 1.26 \times 10^{-6} \text{ kg m}^{-3}, \quad c_0 \approx 2.80 \times 10^{-6} \text{ kg m}^{-3},\\
t_0 \approx 9990 \text{ s}, \qquad h_0 \approx 1.40 \times 10^{-7} \text{ m}.
\end{gathered}
\tag{2.22}
$$

The value of p_0 is in reasonable agreement with estimates of 0.13–0.26 Pa for the partial vapor pressure of water at the poles (Ivanov and Muhleman (2000)). The temperature scale is also in agreement with estimated summer temperatures at the north pole of 200–220 K (Hvidberg (2003)) and 205 K (Zuber et al. (1998)).

From the above values, we calculate $\lambda = 3.77 \times 10^{-4}$. As $\lambda \ll 1$, we can simplify equation $(2.20)_1$ to

$$I\,(1 - a(\phi)) = \gamma(c)T^4. \tag{2.23}$$

We also calculate $\beta \approx 31.0$.

Both the time and height scales (equation (2.22)) are small. This is because, in the absence of transport terms, we have no choice about how to balance the terms in the differential equations (2.15)–(2.17). We therefore look at a typical time and space scale over which the sublimation kinetics occur, and we would expect sublimation to occur in a thin layer over a short time scale. However, we are interested in the long-term behavior of the ice cap. In the section below we rescale both the time and height to obtain values that are more appropriate. However, although the scale for s in (2.22) is small, it is $O(\text{mm a}^{-1})$, which is comparable to an erosion rate on Earth.

2.2. Simplification of the model. There are only two parameters in the model, β and λ, of which the latter is small, so that we may neglect it. Note also that since $\phi = \alpha(t)$ when $s < 0$, we may replace α by ϕ in the differential equations for ρ and c, and also in the definition of m. Define

$$\rho^*(T) = \frac{p_{\text{sat}}}{T} = \frac{1}{T}\exp\left[\beta\left(1 - \frac{1}{T}\right)\right]; \tag{2.24}$$

then we have

$$\begin{aligned} T^4 &= \frac{I[1 - a(\phi)]}{\gamma(c)}, \\ s &= \frac{|u|(\rho^* - \rho)}{1 - \phi}. \end{aligned} \tag{2.25}$$

Thus $T = T(\phi, c)$ and hence $s = s(\phi, c, \rho)$.

The differential equations for h, ρ, and c are

$$\begin{aligned} \frac{dh}{dt} &= -s, \\ \frac{d\rho}{dt} &= (1 - \phi)s, \\ \frac{dc}{dt} &= \phi s\,; \end{aligned} \tag{2.26}$$

these admit the conservation law

$$c + \rho + h = h^*, \tag{2.27}$$

where h^* is constant.

Now we consider the awkward history-dependent recipe for ϕ. Note first that $\frac{dc}{dh} = -\phi$, so that at least for $s < 0$, i.e., while h is increasing, we have $\phi = \alpha = \frac{c}{c+\rho} = \frac{c}{h^* - h}$, and thus

$$c = \phi(h^* - h), \tag{2.28}$$

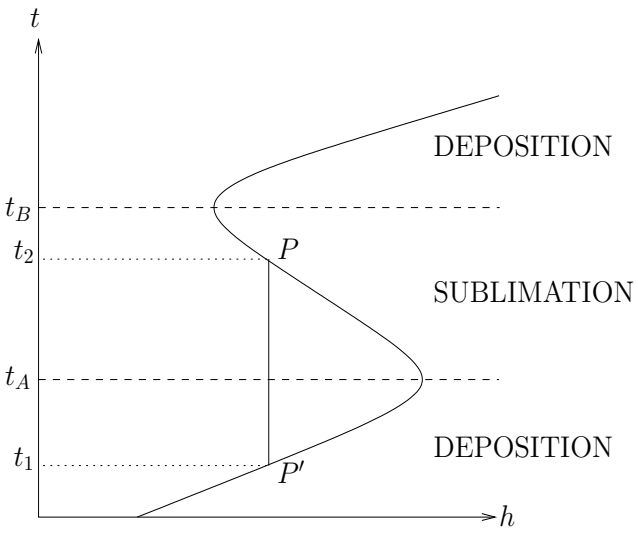

FIG. 2.2. *Calculation of ϕ for $s > 0$ and $s < 0$ for a typical evolution of h.*

and $\phi = \phi_0$ is constant while it is snowing. Suppose that h evolves as in Figure 2.2, i.e., $h > h(0)$. For $0 < t < t_A$, $s < 0$ and thus $\phi = \alpha$ is constant. Now for $t_A < t < t_B$, $s > 0$ and so ϕ at P, for example, is equal to the value of α at P', and this is just the constant ϕ_0. Carrying on in this fashion, we see that in fact ϕ is constant for all t, so that (2.28) applies always.

The argument fails if h decreases below $h(0)$, for the initial condition for ϕ can be arbitrary. But if this happens, ϕ simply switches to the value of ϕ appropriate to the minimum value of h, and is thereafter constant at this value. This argument can be followed through for any choice of $\alpha(c, \rho)$, since the conservation law (2.27) then implies $\alpha = \alpha(c, h)$, and it also applies so long as c and h satisfy ordinary differential equations of the form $\dot{c} = f(c, h)$, $\dot{h} = g(c, h)$; in other words, the argument does not rely on the precise form of (2.26).

Taking now $c(h)$ from (2.28), (2.27) implies

$$\rho = (1 - \phi)(h^* - h), \tag{2.29}$$

whence

$$\rho = \frac{(1 - \phi)c}{\phi}, \tag{2.30}$$

and the model collapses to the single equation

$$\frac{dc}{dt} = \phi\, s(c, I), \tag{2.31}$$

where the sublimation flux is given by

$$s = |u| \left[\frac{\rho^*(c)}{1 - \phi} - \frac{c}{\phi} \right], \tag{2.32}$$

and ρ^* is given by

$$\rho^* = \frac{1}{T} \exp\left[\beta \left(1 - \frac{1}{T} \right) \right], \quad T^4 = IA(\phi)G(c), \tag{2.33}$$

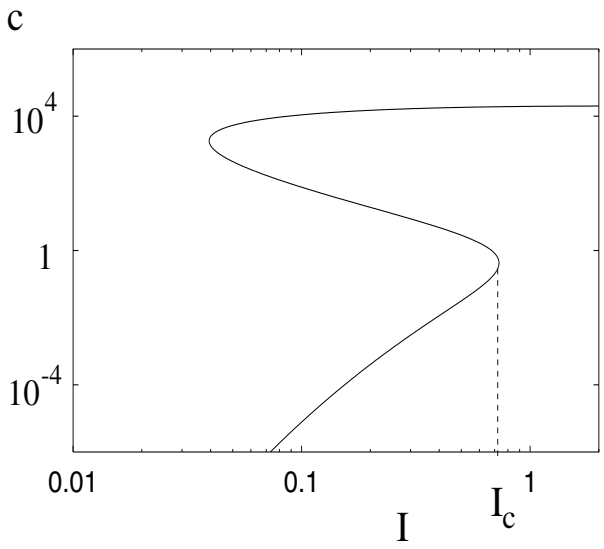

FIG. 2.3. *Equilibrium values of c as a function of the radiative flux I for parameters* $\beta = 15$, $\phi = 0.2$, $\hat{\alpha} = 0.6$, $g = 1.0$ *in the functions* $A = 1 + \hat{\alpha}\phi$, $G = 1 + gc$. *Sublimative runaway occurs for* $I > 0.73$. *Note the logarithmic scale for c.*

where we have defined

$$A = 1 - a, \quad G = \frac{1}{\gamma}. \tag{2.34}$$

A is an increasing function of ϕ, and G is an increasing function of c.

Equation (2.31) is essentially that describing thermal runaway in combustion, and it has multiple equilibria, depending on the values of the parameters. If we use I as an input parameter, then we obtain the equilibria of c in terms of I as shown in Figure 2.3. Note the extreme values of c. These are due to the large value of β. The lower ("cool") and upper ("hot") branches are stable. Sublimative runaway occurs when the insolation I increases beyond the values I_c indicated in the figure.

We can use the large value of β to obtain an approximate expression for I_c. The nose of the curve occurs when $T \approx 1$, and thus, if we define

$$A = 1 + \hat{\alpha}\phi, \quad G = 1 + gc, \quad I = 1 + \hat{I}, \tag{2.35}$$

then we have

$$T \approx 1 + \tfrac{1}{4}(gc + \hat{\alpha}\phi + \hat{I}), \tag{2.36}$$

and thus

$$\rho^* \approx \exp\left[\tfrac{1}{4}\beta(gc + \hat{\alpha}\phi + \hat{I})\right]. \tag{2.37}$$

After a little algebra, we find that the nose of the curve $s = 0$ is given by

$$c \exp\left\{-\tfrac{1}{4}\beta g c\right\} \approx \frac{\phi}{1-\phi} \exp\left[\tfrac{1}{4}\beta(\hat{\alpha}\phi + \hat{I})\right], \tag{2.38}$$

and thus runaway occurs for

$$I > I_c \approx 1 - \hat{\alpha}\phi - \frac{4}{\beta}\left[\ln\left\{\frac{\beta g \phi}{4(1-\phi)}\right\} + 1\right]. \tag{2.39}$$

For the values used in Figure 2.3, this gives $I_c \approx 0.63$, as opposed to the actual value 0.73.

Instability is promoted for larger insolation rates, large dust-albedo coefficient, or large dust fraction in ice. Dustiness is one of the distinguishing features of the Martian atmosphere.

3. Mechanisms of transport. In order to study the effect of this sublimative runaway mechanism in a spatially distributed system, we need to describe transport terms. There are two obvious transport mechanisms. These are the flow of the ice cap itself by viscous creep processes, and the atmospheric surface winds. We discuss each of these in turn.

Katabatic winds are hydraulic flows driven down a cold glacial slope by negative thermal buoyancy. The necessary theory to describe them can be found in several places (e.g., Ball (1956), Nappo and Rao (1987), van den Broeke (1997), Grisogono and Oerlemans (2001)). However, for simplicity we model the summer wind as a constant velocity downslope katabatic wind.

Wind can transport dust, and ice flow can transport ice. The standard shallow ice flow model for ice sheet flow uses lubrication theory and a flow law of Glen type (Paterson (1994)) to predict, in two dimensions, an ice flux of

$$q_i \propto -h^{n+2}|h_x|^{n-1}h_x, \tag{3.1}$$

where n is the exponent in the flow law (Fowler (1992)). This calculation assumes an isothermal ice cap, but is easily modified for a thermally conducting ice cap at low velocities. For conditions appropriate to Mars, typical surface ice velocities are calculated to lie in the approximate range 1–10 mm a^{-1} (Hvidberg (2003)). Therefore, the reduced Péclet number is given by

$$\mathrm{Pe} \sim \frac{u_i d^2}{l\kappa} \sim 3 \times 10^{-3}, \tag{3.2}$$

where u_i is a typical ice velocity of 10 mm a^{-1}, $\kappa = 38$ m^2 a^{-1} is the diffusion coefficient of heat in ice, and l is the horizontal length scale (see below). As the reduced Péclet number is small, this confirms that heat transfer is primarily by conduction in the vertical.

However, for simplicity we model ice transport by a simple diffusion term. In this way, we pose the model of sublimation with transport as

$$\begin{aligned} h_t &= -s + h_{xx}, \\ \nu c_t + u c_x &= \phi s, \end{aligned} \tag{3.3}$$

where u is the constant wind speed and we have now nondimensionalized using the time scale over which the ice moves (t_i). The corresponding depth scale is $h_i = h_0/\nu$ where $\nu = \frac{t_0}{t_i}$, which is a measure of the ratio of ice speed to wind speed, and is of order 10^{-11}, for ice speeds of 10 mm a^{-1} and wind speeds of 30 m s^{-1}. As $\nu \ll 1$, we neglect the time derivative in the equation for c and solve

$$\begin{aligned} h_t &= -s + h_{xx}, \\ u c_x &= \phi s. \end{aligned} \tag{3.4}$$

The new dimensional depth scale is $h_0/\nu \sim 2200$ m, and the time scale is $t_0/\nu \sim 1.58 \times 10^{14}$ s ~ 5 Myr, which are appropriate scales for the evolution of the ice cap

(as we expect, since it is presumably controlled by sublimation–deposition balance). The horizontal length scale l is defined by

$$l = \frac{du_0 c_0}{\rho_s s_0} \approx 50 \text{ km}, \tag{3.5}$$

an appropriate scale for the width of a trough.

Although its derivation when there is transport is more opaque, we will continue to assume that sublimation can be written as a function $s(c, I)$ having a general form akin to (2.32). The important feedback mechanism in the model is the dependence of the sublimation flux on insolation. We let x measure distance from the pole, so $h_x < 0$. The dimensionless radiation flux received at the surface is approximately

$$I = 1 - \mu h_x, \tag{3.6}$$

where

$$\mu = \frac{h_0 \tan \theta_f}{l}. \tag{3.7}$$

Using the values above, we estimate $\mu \sim 0.2$.

This small dependence is amplified by the strong dependence of saturation vapor pressure on temperature. Using the approximation of (2.37) in (2.32), we have

$$s \approx \hat{A} e^{pc - n h_x} - Bc, \tag{3.8}$$

where

$$\hat{A} = \frac{|u|}{1-\phi} \exp\left(\tfrac{1}{4}\hat{\alpha}\beta\phi\right), \quad p = \tfrac{1}{4}\beta g,$$
$$n = \tfrac{1}{4}\beta\mu, \quad B = \frac{|u|}{\phi}. \tag{3.9}$$

With $\beta = 31$, the value of n is about 1.5.

This approximation fails to represent the eventual decline of s at large c as implied by (2.32) and (2.33), and so as a model problem we define

$$s = f(c) - n h_x, \tag{3.10}$$

where $f(c)$ has the cubic shape shown in Figure 3.1. To be specific, we choose

$$f(c) = (c-1)(c-2)\Big(1 - \frac{c}{M}\Big), \tag{3.11}$$

which mimics the expression in (2.32), providing $M \gg 1$.

In reality, the location of the right-hand boundary of the ice cap is determined by the evolution of the ice cap, and so this is a free boundary problem. However, for simplicity we fix the right-hand edge of the ice cap by requiring

$$h = 0 \quad \text{at} \quad x = L, \tag{3.12}$$

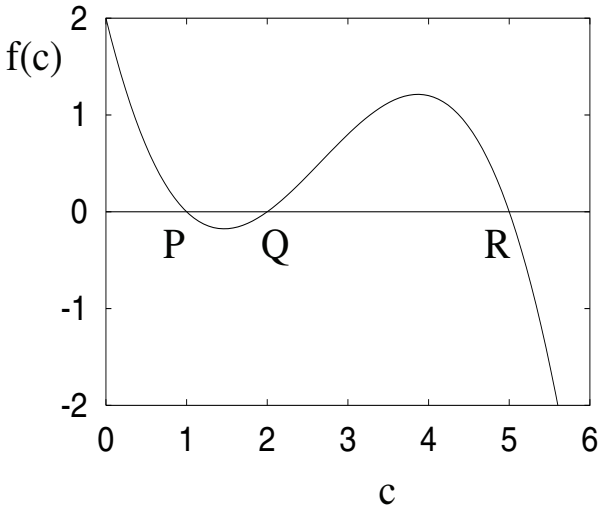

FIG. 3.1. *The function* $f(c) = (c-1)(c-2)\left(1-\frac{c}{M}\right)$, *with* $M = 5$.

where

$$L = \frac{w}{l}, \tag{3.13}$$

and w is the half-width of the ice cap. Experience with modeling terrestrial ice sheets (Fowler (1992)) does not suggest that this will have a serious dynamic effect on the behavior of the solutions. For the Martian north polar ice cap, $w = 500$ km, and so using the value for l given in (3.5), we calculate that $L = 10$.

We require the ice cap to be symmetric about the pole, and so

$$h_x = 0 \quad \text{at} \quad x = 0. \tag{3.14}$$

Only one boundary condition is required for c; we choose to prescribe c at the pole,

$$c = c_0(t) \quad \text{at} \quad x = 0, \tag{3.15}$$

for some function $c_0(t)$. We discuss some specific choices of the function $c_0(t)$ below, but note that there is no data that can be used to prescribe c at the pole.

The system of equations in (3.4) coupled with (3.10) has steady solutions of constant slope, e.g., $h = \hat{h}(1 - \frac{x}{L})$, providing $s = 0$ and thus $c = \hat{c}$, where

$$f(\hat{c}) + \frac{n\hat{h}}{L} = 0. \tag{3.16}$$

Such a steady state does not satisfy the symmetry condition at the summit, and we anticipate that there will be an adjustment region close to the summit to accommodate this condition.

Stability. We expect that the wavelength of traveling waves on the ice cap surface will be less than the length of the ice cap, and therefore do not seek to satisfy the boundary conditions given by (3.12), (3.14), and (3.15) in the analysis below.

We linearize the system of equations (3.4) and (3.10) about the straight line steady state given above by setting

$$h = \hat{h}\left(1 - \frac{x}{L}\right) + H\exp(\sigma t + ikx), \tag{3.17}$$

$$c = \hat{c} + C\exp(\sigma t + ikx), \tag{3.18}$$

$$s = S\exp(\sigma t + ikx), \tag{3.19}$$

where H, C, and S are small in comparison with the steady state values. We find that the growth rate and wave speed are, respectively,

$$\text{Re }\sigma = -k^2 + \frac{n\omega k^2}{\omega^2 + k^2}, \tag{3.20}$$

$$-\frac{\text{Im }\sigma}{k} = -\frac{nk^2}{\omega^2 + k^2}, \tag{3.21}$$

where $\omega = \frac{\phi f'}{u}$. Instability occurs for $\text{Re}(\sigma) > 0$: from (3.20) this will be where $\omega(n-\omega) > 0$, or equivalently where $0 < \omega < n$. Note that $\omega > 0$ indicates that in the steady state $f'(\hat{c}) > 0$. From (3.21), the wave speed is always negative, and so waves will travel polewards.

If $\text{Re}(\sigma) > 0$, we can calculate the most unstable wavenumber k_m using (3.20) to be

$$k_m^2 = \omega\left(\sqrt{n\omega} - \omega\right). \tag{3.22}$$

The requirement that k_m be real implies that $n > \omega$; this is always the case because it is the criterion for instability to occur. We therefore conclude that a steady state in which $f' > 0$ may be linearly unstable to traveling waves of finite wavelength.

Traveling waves. As the steady state may be linearly unstable to finite amplitude traveling waves, we look for such solutions directly. Thus we put

$$h = h(\xi), \quad c = c(\xi), \tag{3.23}$$

where the traveling wave variable is

$$\xi = x + vt, \tag{3.24}$$

and we expect, but do not assume, that $v > 0$. The linear result above would in fact suggest that $0 < v < n$. Substituting (3.23) into equations (3.4) yields the pair of ordinary differential equations

$$\begin{aligned} b' &= vb - s, \\ uc' &= \phi s, \end{aligned} \tag{3.25}$$

in which $b = -h'$ and $s = s(c, b)$. These equations can therefore be simply analyzed in the (c, b) phase plane.

We consider as a generic example the case where $s = f(c) + nb$, and we denote the steady states as P, Q, R, as shown in Figure 3.1. The results are then the following. When $0 < v < n$, P and R are saddles, while Q is a node or spiral, which undergoes a Hopf bifurcation at

$$v = v_c = n - \frac{\phi f'}{u}, \tag{3.26}$$

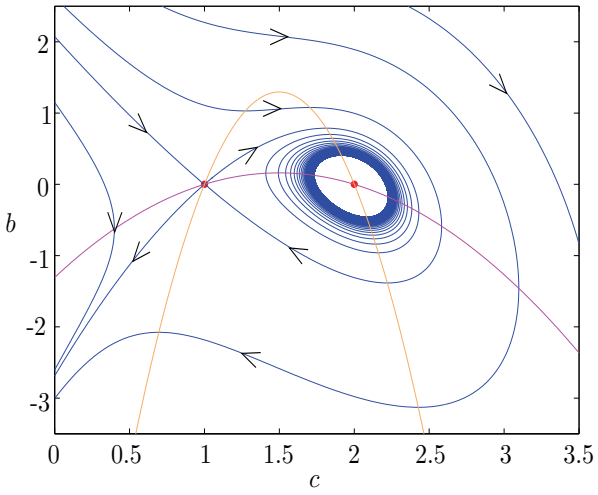

FIG. 3.2. *Phase plane of equations* (3.25). *Parameter values used were* $\phi = 0.2$, $n = 1.53$, $c_1 = 1$, $c_2 = 2$, $M = 100$, $u = 1$, *and* $V = 1.34$. *The orange and magenta dashed lines are the nullclines; arrows show trajectory direction. (Color version available online.) The steady states at* $(1, 0)$ *and* $(100, 0)$ *are saddle points, while that at* $(2, 0)$ *is an unstable spiral about which there is a limit cycle.*

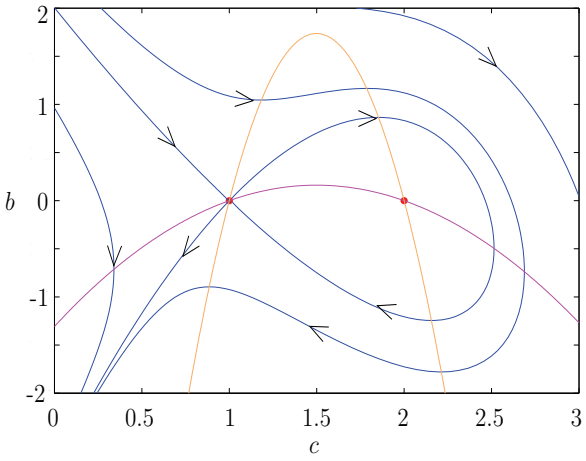

FIG. 3.3. *Phase plane of equations* (3.25) *with parameter values as in Figure* 3.2, *except that* $V = 1.388$. *The limit cycle has become a homoclinic orbit to the saddle point at* $(1, 0)$.

assuming v_c is positive. Q is unstable for $v > v_c$, and numerical computations suggest that the Hopf bifurcation is supercritical, so that there is a stable periodic solution for $v > v_c$. This orbit exists up to a value $v = v_h$, at which it becomes heteroclinic to P, and disappears in a "blue skies" bifurcation (Thompson and Stewart (1986)). The stable orbit and its disappearance are shown in Figures 3.2 and 3.3.

If $v > n$, P and R are still saddles, and Q is an unstable node or spiral. It is

possible that the limit cycle may still exist, and this probably depends on the size of f; it is also possible for the limit cycle to disappear by coalescence with R, but this seems unlikely for large R. In fact, it is found that as $M \to \infty$ in (3.11), the limit cycle remains finite and independent of M. This indicates that the limit cycle for the actual definition of s can be suitably computed using the large β approximation (3.8), i.e.,

$$s(c, b) \approx Ae^{pc+nb} - Bc, \tag{3.27}$$

where the constants are given by (3.9). Computation of solutions using (3.27) shows that the limit cycle which appears is generally unstable. This does not necessarily imply that the underlying traveling wave is unstable, however.

In general, one expects to see traveling waves in systems such as reaction-diffusion equations when a steady state has an oscillatory instability. In particular, systems whose kinetics admit a Hopf bifurcation will generally possess traveling wave solutions, and the stability of these solutions can be expected to be associated with the issue of whether the Hopf bifurcation is subcritical or supercritical. In the present case, because traveling waves exist only in the neighborhood of a fixed point (Q) which is directly unstable, it is to be expected that the traveling waves we have found will also be unstable, and indeed this appears to be confirmed by numerical solution of the full equations.

Numerical solution. To obtain numerical solutions to the system of equations (3.4) and (3.10), we implemented a numerical method in Fortran 77. We used an implicit finite difference scheme to evolve h in time and an improved Euler method to solve the quadrature for c. At the boundaries, we used second order accurate approximations for the height and slope.

Steady state ice cap profiles were calculated using a constant boundary value for the suspended dust concentration at the summit; i.e., the boundary condition for c in (3.15) is given by $c_0(t) = c_0$, where c_0 is constant. To obtain a steady state profile comparable to that of the current day ice cap, we first note that the scale for h is 2200 m, while the current day ice cap elevation at the pole is approximately 3000 m (Zuber et al. (1998)). This indicates that, dimensionlessly, $h(0) \approx 1.36$.

Using this value, we calculated the straight line approximation to the steady state described above; this approximation was then used as the initial condition for h. We also calculated the three corresponding constant values of c in the steady state away from the summit and used these as the boundary values c_0: $c_0 = 1.34$, 1.65, and 20.0122.

The resulting steady state profiles of h for each boundary value c_0 are shown in Figure 3.4. For all three values of c_0 a steady state is attained that has constant slope away from the pole. Close to the pole there is a correction region due to the symmetry condition, (3.14). We see that is possible to produce a physically realistic steady state shape profile for different boundary values c_0. In the two uppermost plots, this steady state is very close to the initial condition (which was a straight line passing through $(0, 1.36)$ and $(10, 0)$).

In the lowest plot, where c_0 is close to $M = 20$, the steady state is not close to the initial condition. This is because close to M the value of $f(c)$, and therefore the value of s, is more sensitive to changes in c. This means that the change in c across the correction region near the pole has a larger effect on $f(c)$ and, from (3.10), it therefore has a larger effect on the resulting h profile. From the numerical solutions it is verified that away from the pole $s = 0$ in the steady states. The same qualitative

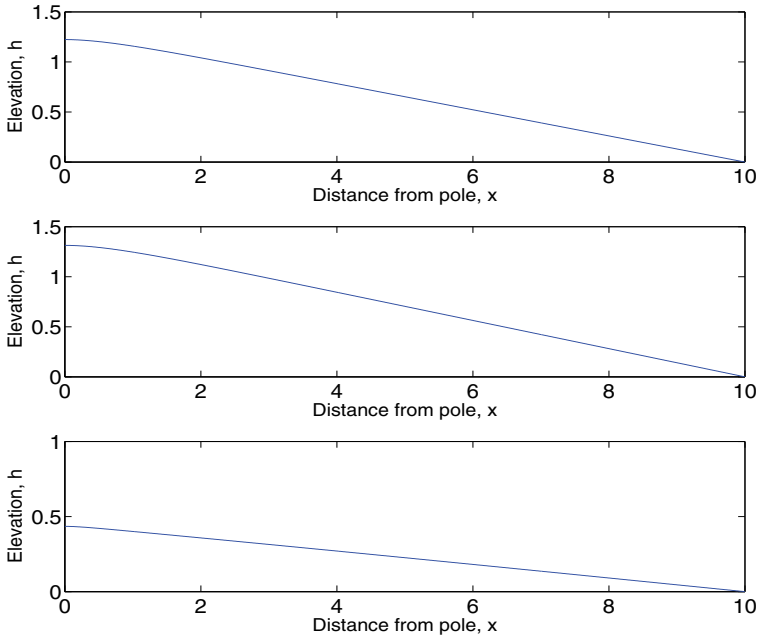

FIG. 3.4. *Steady state profiles of h with $c = c_0$ at $x = 0$. The upper plot shows the solution for $c_0 = 1.34$, the central plot for $c_0 = 1.65$, and the lower plot for $c_0 = 20.0122$. Parameter values used were $\phi = 0.2$, $u = 1$, $n = 1.53$, $c_1 = 1$, $c_2 = 2$, and $M = 20$; in all cases the initial condition for h was a straight line passing through $(0, 1.36)$ and $(10, 0)$. The corresponding constant values of c in the steady state away from the correction region near $x = 0$ were $\hat{c} = 1.31$, 1.62, and 20.0041.*

behavior is seen for larger values of M: the value $M = 20$ was chosen for ease of both illustration and numerical calculation.

All three steady states shown in Figure 3.4 are stable; if this were not the case, they would not be seen numerically. This might seem to contradict the earlier calculation that if c_0 lies on the middle branch of the $f(c)$ curve where $f'(c) > 0$, the steady state is unstable. However, previous analytic calculations did not account for the boundary conditions on h and c, which appear to have a stabilizing effect. Later we see that some steady states where $f'(c_0) > 0$ are indeed unstable.

For $1 < c_0 < 1.85$ and $c_0 > 20$, numerical solutions indicate that a steady state exists with an h profile that has a shape similar to those shown in Figure 3.4: a straight line away from the pole which has positive h everywhere. For $0 < c_0 < 1$ and $7 < c_0 < 20$, a similarly shaped steady state exists, except that the ice cap elevation is negative everywhere. It is not clear what the physical interpretation of negative h is; one possibility is that it represents a situation in which no steady state ice cap is possible.

However, for $1.85 < c_0 < 7$, no steady state profile is found numerically; instead, global oscillations in both c and h occur. This is an indication that the steady state, if it exists, is unstable. These global oscillations have three main phases.

First, as shown in Figure 3.5, there is a phase where c increases from a value close to the boundary value c_0 to an $O(M)$ value, and a polewards-traveling wave in c across the ice cap is observed. A corresponding depression forms on the ice cap surface, which deepens and migrates polewards.

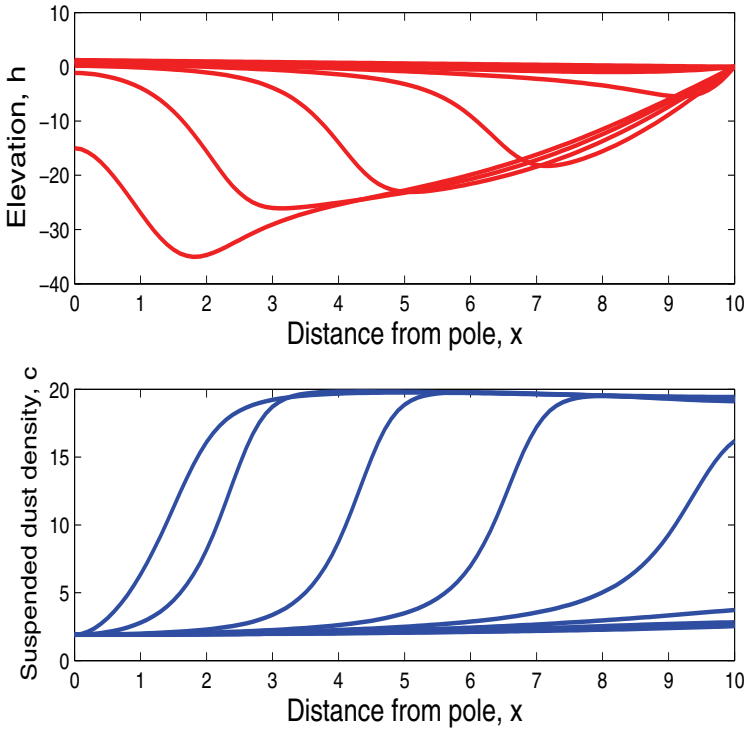

FIG. 3.5. *Numerical calculations of the elevation h and suspended dust density c as a function of distance from the pole, x, with boundary condition $c_0 = 1.9$. The upper plot shows the elevation of the ice cap surface, h, and the lower plot the evolution of the suspended dust density, c. The solution is shown between times $t = 0$ and $t = 4.8$ at time intervals of $t = 0.6$; the wave in c travels from right to left, as does the wave in h. The remaining parameter values are as in Figure* 3.4.

In the second phase shown in Figure 3.6, the wave in c changes direction and moves equatorwards across the ice cap; when this wave reaches the right-hand boundary, c decreases from an $O(M)$ value to an $O(c_0)$ value. The surface depression continues to deepen, but does so less rapidly.

Finally, over a much longer time scale, both the surface elevation and suspended dust density increase back to their initial profiles and the cycle begins again. This final phase is shown in Figure 3.7.

A three-dimensional plot of the c profile of the same oscillation is shown in Figure 3.8; the maximum and minimum values of c as a function of time are shown in Figure 3.9. Both figures have a logarithmic c scale for ease of illustration. Figure 3.8 shows the waves in c moving from the pole to the right-hand boundary (we do not see the polewards traveling waves as they are on the far side of the "bump"). From Figure 3.9 it can be seen that the oscillations are periodic in time and that the traveling waves in c move quickly. Both c and h become negative over some or all of the ice cap, which has no meaningful physical interpretation. If these global oscillations occur, a backwards-traveling wave in c is initiated, as shown in the uppermost plot of Figure 3.5. The effect of this wave in the suspended atmospheric dust is manifested in the corresponding surface profile as a depression that deepens as the wave in c migrates

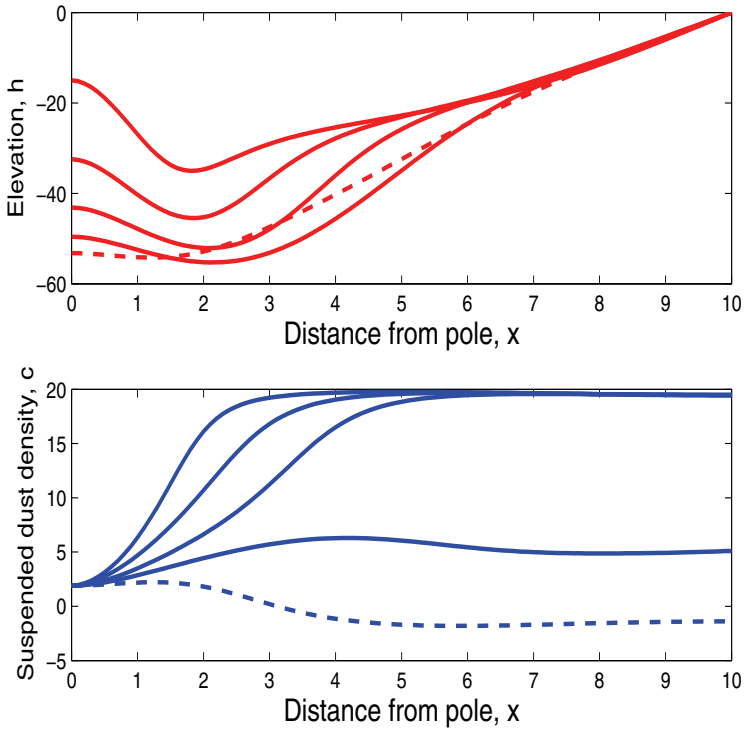

FIG. 3.6. *Numerical calculations of the elevation h and suspended dust density c as a function of distance from the pole, x, with boundary condition $c_0 = 1.9$. The upper plot shows the elevation of the ice cap surface, h, and the lower plot the evolution of the suspended dust density, c. The solution is shown between times $t = 4.8$ and $t = 6.8$ at time intervals of $t = 0.5$; the solution at the final time $t = 6.8$ is shown as a dashed line for ease of illustration. In this case, the surface depression shown in the upper plot is deepening with time, and the wave in c shown in the lower plot is moving from left to right. The remaining parameter values are as in Figure* 3.4.

polewards. Such a depression has a similar shape to a trough, i.e., a steeper equator facing wall.

Although the initial condition for the solution shown in Figures 3.5–3.9 is an approximation to the steady state, in this case there is in fact no steady state ice cap on which the trough can form. However, if c_0 is initially constant at a value close to c_1 for which there is a stable steady state, and then subsequently increases to a value at which global oscillations occur, a trough can form as a surface depression on a steady state ice cap. At later times after the initial transient, global oscillations in c and h occur, as would be seen if c_0 was constant at the end value.

A trough can also form if the boundary condition on c causes a transition between stable steady states (rather than a transition between a stable steady state and the global oscillations described above). One such example is shown in Figure 3.10, where the boundary condition causes a transition between a steady state with positive elevation and one with a negative elevation. At a later time (not shown), h and c reach their steady state profiles.

Such a transition between stable steady states can in fact occur via either a polewards- or an equatorwards-traveling wave. A polewards-traveling wave occurs

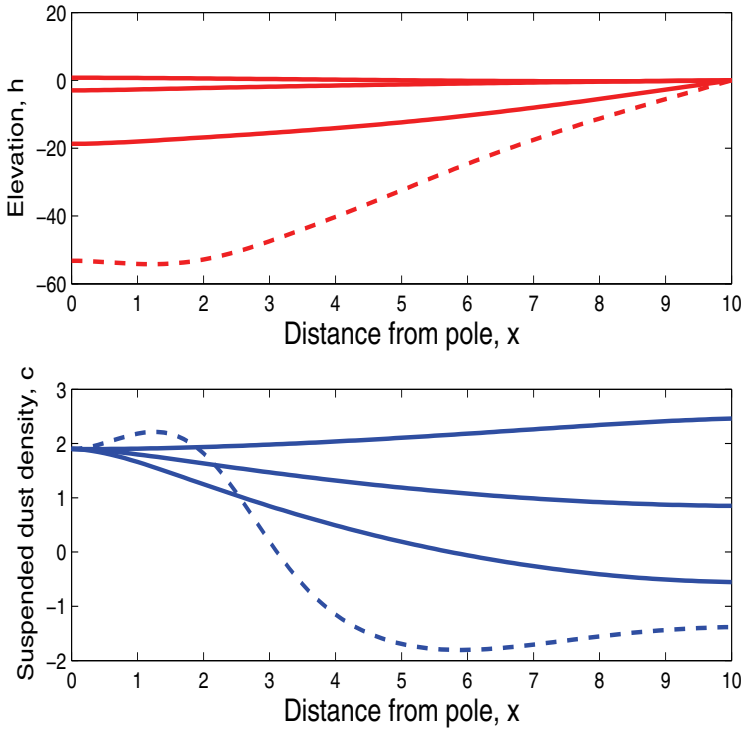

FIG. 3.7. *Numerical calculations of the elevation h and suspended dust density c as a function of distance from the pole, x, with boundary condition $c_0 = 1.9$. The upper plot shows the elevation of the ice cap surface, h, and the lower plot the evolution of the suspended dust density, c. The solution is shown between times $t = 6.8$ and $t = 36.8$ at time intervals of $t = 10$; the solution at the initial time $t = 6.8$ is shown as a dashed line for ease of illustration, and is the same as the final profile indicated by the dashed line in Figure* 3.6. *In this case, both the ice cap surface elevation and the suspended dust density are increasing. The remaining parameter values are as in Figure* 3.4.

if c_0 changes from the lower steady state value to the higher steady state value at the boundary, and an equatorwards-traveling wave occurs if the reverse is true, i.e., c_0 changes from the higher steady state value to the lower steady state value at the boundary. However, for no choice of boundary condition $c_0(t)$ was more than one trough formed on the ice cap surface; it was not possible to obtain a sequence of traveling waves. This indicates that if the traveling wave solutions found in the phase plane analysis exist, they are unstable. However, it seems that the imposed boundary conditions determine the behavior observed in the numerical solutions, and these are not accounted for in the previous analytic work.

Also, once a surface depression has formed on the ice cap surface, the model is no longer valid. This is because the katabatic wind should always flow downslope; therefore, over a portion of the ice cap where $h_x > 0$, the wind should change direction, and it can therefore no longer be assumed that u is constant over the whole ice cap. Another issue is that it is not realistic to prescribe c_0 at the pole, and the choice of $c_0(t)$ is arbitrary, although numerical simulations indicate that an increase in Martian obliquity will cause an increase in the amount of atmospheric dust (Newman, Lewis, and Read (2005)). Therefore, increasing or decreasing c_0 at the pole could be

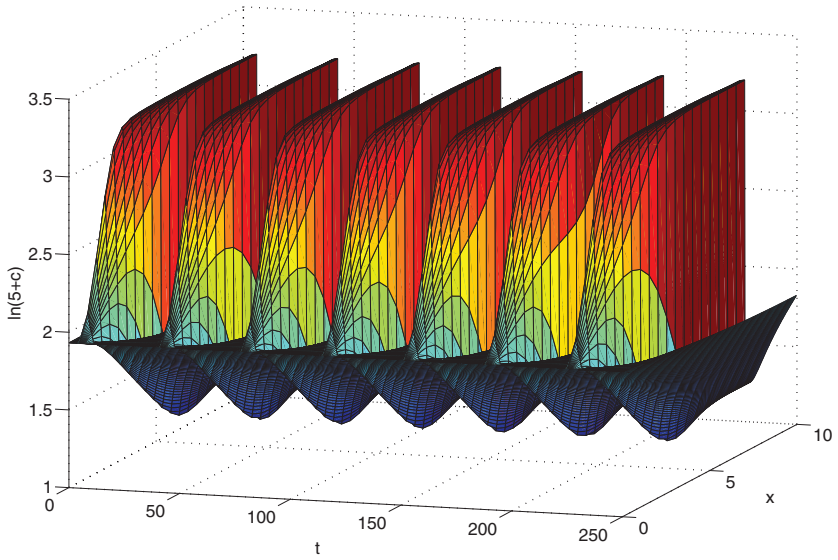

FIG. 3.8. *A three-dimensional surface plot of the suspended dust density as a function of space and time. Note the logarithmic scale on the c axis. The parameter values and boundary conditions used were as in Figure* 3.4. *Red indicates large c values, while blue indicates low c values. The spatial resolution is* 0.5 *space units and the solution is shown from* $t = 0$ *to* $t = 250$ *at intervals of* $t = 0.2$.

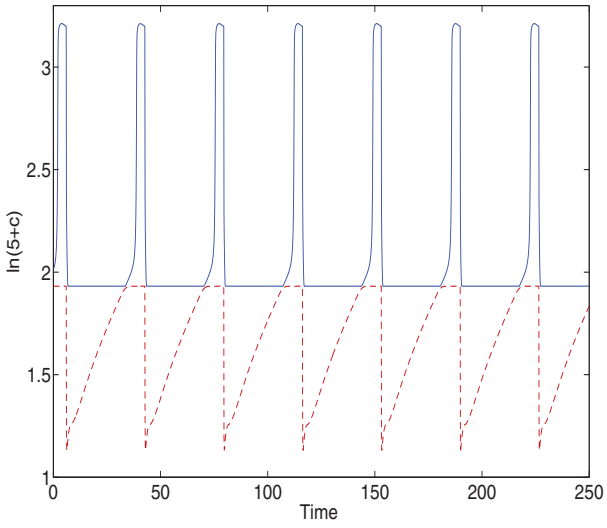

FIG. 3.9. *Numerical calculation of the maximum value of c as a function of time (upper solid line) and the minimum value of c as a function of time (lower dashed line). The parameter values and boundary conditions used were as in Figure* 3.4.

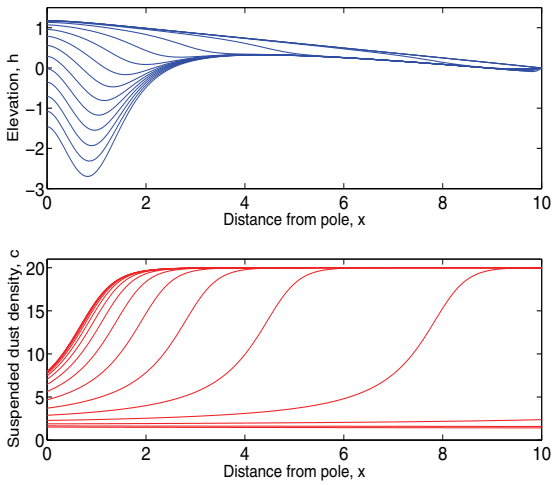

FIG. 3.10. *Numerical solution for h and c as functions of x (upper and lower plots, respectively). The initial condition and parameter values are as in Figure* 3.4*; the boundary condition used was* $c_0 = 1.34 + 0.5(8 - 1.34)\{\tanh[30(t - 0.5)] + 1\}$. *The solution is shown at time intervals of* 0.01 *between* $t = 0.45$ *and* $t = 0.60$. *The waves in c and h travel from right to left.*

physically motivated as a representation of obliquity-induced climate change. Finally, the model allows both h and c to become negative, and this has no meaningful physical interpretation.

On the other hand, the model produces steady state ice cap profiles with a realistic shape, and it allows a single trough to develop for certain choices of boundary condition. This trough typically has the correct shape, i.e., a steeper equator-facing slope, and it is possible to describe some features of such a trough analytically (Zammett (2008)).

4. Conclusions. In this paper, we have derived a mathematical model of the kinetics of ice and dust in the Martian north polar region. This model was based on the description of sublimation kinetics by Ivanov and Muhleman (2000) and on the coupling of these kinetics with water vapor transport by Ng and Zuber (2006), and describes dust-albedo feedback. However, the model presented here explicitly describes dust, both frozen in the ice cap and suspended in the atmosphere above it. We have also included the greenhouse effect of suspended atmospheric dust.

Solutions of the model in the absence of transport terms suggest that multiple equilibria are possible, and that these equilibria can be characterized by the insolation received at the surface and the suspended dust density. We then added transport terms to the model: the transport of atmospheric dust by a downslope katabatic wind and ice transport by steady state creep. We used the simplest mathematical expressions for such processes by including a constant velocity wind and a linear diffusion term to model ice transport. In addition, we supposed that the ice cap margin was fixed, rather than allow it to be a free boundary. This is somewhat equivalent to prescribing an oceanic margin for a terrestrial ice sheet rather than a land-based margin. There is no suggestion that this difference is significant for terrestrial ice sheets, and we do not consider it likely that it will affect the possibility of forming multiple troughs, for example. Finally, we used the results from the kinetic

model to prescribe a function for the sublimation flux. This simplification reduces the model to a pair of coupled partial differential equations for the ice surface elevation and the suspended dust density.

Steady states of this system are possible in which the ice cap elevation is approximately a straight line and the suspended dust density has a constant value across the ice cap away from the pole. Linear stability analysis suggests that such a steady state may be linearly unstable, and phase plane analysis shows that traveling wave solutions are possible.

However, no such traveling waves are seen in the numerical solutions, suggesting that if such waves exist, they are always unstable. Instead, it is possible to generate solitary traveling waves in the suspended atmospheric dust density, and such a wave causes a depression in the ice cap surface to form. These waves in the suspended dust density are generated by changing the boundary condition on the suspended dust density at the pole as a function of time. This could be interpreted as a change in the dustiness of the Martian atmosphere caused by a change in climate. Therefore, in this model, a single trough may form, but there are no stable traveling waves as in the model of Ng and Zuber (2006), and multiple troughs are not seen in the model. This suggests that the troughs do not form as a patterning instability if the katabatic wind velocity is assumed to be constant, contradicting the prediction of Ng and Zuber (2006).

However, the model as it stands requires modification if it is to accurately describe processes occurring in the Martian north polar region. First, it may not be realistic to prescribe the suspended dust density at the summit, and it is this boundary condition which determines the features of the numerical solution. As mentioned above, a katabatic wind should always flow downslope; when a depression has formed on the ice cap surface, the assumption of a constant velocity wind is no longer valid. When these problems are rectified, we find that an improved model does in fact allow multiple troughs to form in certain circumstances (Zammett (2008)).

In a two-dimensional model such as this, we are unable to address the issue of the spiral form of the troughs. In reaction-diffusion systems, the breaking of symmetry of target patterns to form spiral waves may be associated with the finite size of dust particles which are able to "fix" a rotating periodic oscillation on their surfaces. In the present case, we might suppose symmetry breaking could occur if the troughs propagate inwards, so that the margins act as the nucleation zones. This is entirely speculative, of course, but somewhat consistent with the inward propagation shown in Figure 3.10.

Acknowledgment. The authors are indebted to Felix Ng for sharing his observations and insights. R. J. Z. acknowledges the support of an EPSRC studentship, and A. C. F. acknowledges the support of the Mathematics Applications Consortium for Science and Industry (http://www.macsi.ul.ie) funded by the Science Foundation Ireland mathematics initiative grant 06/MI/005.

REFERENCES

V. Baker (2001), *Water and the Martian landscape*, Nature, 412, pp. 228–236.

F. K. Ball (1956), *The theory of strong katabatic winds*, Aust. J. Phys., 9, pp. 373–386.

K. R. Blasius, J. A. Cutts, and A. D. Howard (1982), *Topography and stratigraphy of Martian polar layered deposits*, Icarus, 50, pp. 140–160.

M. H. Carr (1982), *Periodic climate change on Mars: Review of evidence and effects on distribution of volatiles*, Icarus, 50, pp. 129–139.

S. M. Clifford (1987), *Polar basal melting on Mars*, J. Geophys. Res., 92, pp. 9135–9182.
S. M. Clifford (1993), *A model for the hydrologic and climatic behavior of water on Mars*, J. Geophys. Res., 98, pp. 10,973–11,016.
J. A. Cutts and B. H. Lewis (1982), *Models of climate cycles recorded in Martian polar layered deposits*, Icarus, 50, pp. 216–244.
D. A. Fisher (1993), *If Martian ice caps flow: Ablation mechanisms and appearance*, Icarus, 105, pp. 501–511.
D. A. Fisher (2000), *Internal layers in an "accublation" ice cap: A test for flow*, Icarus, 144, pp. 289–294.
A. C. Fowler (1992), *Modelling ice sheet dynamics*, Geophys. Astrophys. Fluid Dyn., 63, pp. 29–65.
R. Greeley, N. Lancaster, S. Lee, and P. Thomas (1992), *Martian aeolian processes, sediments, and features*, in Mars, H. H. Kieffer, B. M. Jakosky, C. W. Snyder, and M. S. Mathews, eds., University of Arizona Press, Tucson, AZ, pp. 730–766.
B. Grisogono and J. Oerlemans (2001), *Katabatic flow: Analytic solution for gradually varying eddy diffusivities*, J. Atmos. Sci., 58, pp. 3349–3354.
A. D. Howard (1978), *Origin of the stepped topography of the Martian poles*, Icarus, 34, pp. 581–599.
A. D. Howard (1981), *Effect of wind on scarp evolution on the Martian poles*, in Reports of Planetary Geology Program, NASA, pp. 333–335.
A. D. Howard (2000), *The role of eolian processes in forming surface features of the Martian polar layered deposits*, Icarus, 144, pp. 267–288.
A. D. Howard, J. A. Cutts, and K. R. Blasius (1982), *Stratigraphic relationships within Martian polar cap deposits*, Icarus, 50, pp. 161–215.
C. C. Hvidberg (2003), *Relationship between topography and flow in the north polar cap on Mars*, Ann. Glaciol., 37, pp. 363–369.
A. B. Ivanov and D. O. Muhleman (2000), *The role of sublimation for the formation of the Northern ice cap: Results from the Mars Orbiter Laser Altimeter*, Icarus, 144, pp. 436–448.
H. H. Kieffer, S. C. Chase, Jr., T. Z. Martin, E. D. Miner, and F. D. Palluconi (1976), *Martian north pole summer temperatures: Dirty water ice*, Science, 194, pp. 1341–1344.
C. Leovy (2001), *Weather and climate on Mars*, Nature, 412, pp. 245–249.
K. N. Liou (2002), *An Introduction to Atmospheric Radiation*, 2nd ed., Academic Press, San Diego, CA.
J. D. Murray (1993), *Mathematical Biology*, 2nd ed., Springer-Verlag, Berlin.
C. J. Nappo and K. S. Rao (1987), *A model study of pure katabatic flows*, Tellus, 39A, pp. 61–71.
C. E. Newman, S. R. Lewis, and P. L. Read (2005), *The atmospheric circulation and dust activity in different orbital epochs on Mars*, Icarus, 174, pp. 135–160.
F. S. L. Ng and M. T. Zuber (2006), *Patterning instability on the Mars polar ice caps*, J. Geophys. Res., 111, article E02005.
W. S. B. Paterson (1994), *The Physics of Glaciers*, 3rd ed., Pergamon, Oxford, UK.
J. D. Pelletier (2004), *How do spiral troughs form on Mars?*, Geology, 32, pp. 365–367.
J. B. Pollack, D. S. Colburn, F. M. Flasar, C. E. Carlston, and D. Pidek (1979), *Properties and effects of dust particles suspended in the Martian atmosphere*, J. Geophys. Res., 84, pp. 2929–2945.
P. Thomas, S. Squyres, K. Herkenhoff, A. Howard, and B. Murray (1992), *Polar deposits of Mars*, in Mars, H. H. Kieffer, B. M. Jakosky, C. W. Snyder, and M. S. Mathews, eds., University of Arizona Press, Tucson, AZ, pp. 767–795.
J. M. T. Thompson and H. B. Stewart (1986), *Nonlinear Dynamics and Chaos*, John Wiley, Chichester, UK.
O. B. Toon, J. B. Pollack, W. Ward, J. A. Burns, and K. Bilski (1980), *The astronomical theory of climate change on Mars*, Icarus, 44, pp. 552–607.
H. Tsoar, R. Greeley, and A. R. Peterfreund (1979), *Mars: The North polar sand sea and related wind patterns*, J. Geophys. Res., 84, pp. 8167–8181.
D. Tyler, Jr. and J. R. Barnes (2005), *A mesoscale model study of summertime atmospheric circulations in the north polar region of Mars*, J. Geophys. Res., 110, article E06007.
M. van den Broeke (1997), *Momentum, heat and moisture budgets of the katabatic wind layer over a mid-latitude glacier in summer*, J. Appl. Meteorol., 36, pp. 763–774.
R. J. Zammett (2008), *Gravity Currents on Earth and Mars*, D.Phil Thesis, Mathematical Institute, University of Oxford, Oxford, UK.
M. T. Zuber et al. (1998), *Observations of the north polar region of Mars from the Mars Orbiter Laser Altimeter*, Science, 282, pp. 2053–2060.